Geometrically Kinetic Competition Mechanism to Shape Control on Digenite Nanocrystals with Silica Vapor in APCVD

Hao-Xu Zhang,[†,‡] Jian-Ping Ge,[†] and Ya-Dong Li*[,†]

Department of Chemistry, Tsinghua University, Beijing 100084, P. R. China and Institute of Physics, Chinese Academy of Sciences, Beijing 100080, P. R. China

Received: April 16, 2006; In Final Form: May 26, 2006

We report shape control synthesis of digenite nanosheets (growing perpendicular to the ⟨111⟩ direction) and nanowires (growing along the ⟨111⟩ direction) through control on the silica vapor pressure in the system. Critical vapor pressures for silica sheath initialization and crystal shape maintenance are determined in two sets of experiments. The geometrically kinetic competition (GKC) mechanism, which was first proposed in our former work (*J. Phys. Chem. B* **2005**, *109*, 11585), is also supposed to be responsible for the phenomenon reported here.

Introduction

As a key to understanding the mechanism for shape control synthesis of nanocrystals with various templates, such as oxides in chemical vapor deposition,[1−9] Au nanoparticles in vapor−liquid−solid or vapor−solid growth of nanowires,[10−12] and surfactant molecules in solution synthesis,[13−17] the interaction between the template material and the core at the interface is of great interest. In the past few years, several excellent works have been published, dealing with the problem. Zhang and co-workers reported how surface charge had dominated the formation of titanate nanotubes.[18,19] Wang and co-workers successfully explained how the growth of ZnO nanohelixes and nanosprings was governed by polar surfaces.[20−22] Saponjic and co-workers theoretically analyzed how positive charging unscrolls TiO_2 nanotubes.[23] While Schmidt and co-workers calculated the surface energy and interface energy in the Au-cluster−Si-nanowire system and explained the phenomenon that the vapor−liqiud−solid grown Si nanowires change the growth direction from ⟨111⟩ to ⟨110⟩ at a crossover diameter of about 20 nm.[24] Most recently, Manna et al. did an interesting first-principle analysis on unpassivated and surfactant-passivated wurtrite CdSe crystals and pointed out that 0001Cd and $000\bar{1}$Cd facets can rationalize anisotropic growth of CdSe nanocrystals.[25]

Oxides have proved to be very useful template materials for oxide-assisted growth (OAG) of nanowires and nanobelts in the past few years.[1−9] Wang et al. successfully grew monoclinic Cu_2S nanowires with the aid of simultaneously formed thin oxide layers on the nanowires.[5] Tang et al. grew In nanowires by employing MgO as the shell material.[6] Lee and co-workers developed the method by successful synthesis of nanowire/nanobelts of a host of materials, including Si,[1] Ge,[2] SiC,[7] SnO_2,[8] and GaN.[9] Furthermore, on the basis of the ab initio analysis on the structural and chemical properties of Si_mO_n clusters,[26] they explained the mechanism for nucleation and growth of the Si nanowires. In our works, however, we focused our attention on the interaction between the sheath (SiO_2) and core (Bi_2S_3[4a] and Fe_7S_8[4b]) materials, which is crucial for understanding and predicting the growth behavior. In the case of Bi_2S_3,[4a] we attributed the successful synthesis of silica-sheathed nanowires at an extraordinarily high temperature of 650 °C to selective adsorption of silica species on Bi(1) sites through the oxygen bridges. In addition, in the case of Fe_7S_8,[4b] we proposed a hypothesis of geometrically kinetic competition (GKC) for the first time to explain the phenomenon of silica vapor-pressure-dependent growth, that is, when the silica vapor pressure is low, the Fe_7S_8 crystals tend to grow perpendicular to the *c* axis but when water vapor was introduced into the system to increase the silica vapor pressure the Fe_7S_8 crystals change to grow along the *c* axis. Moreover, we observed further support to our hypothesis from experimental results about the turning angles on a silica-sheathed Fe_7S_8 nanowire, which match our predictions fairly well.[4b] Here we show another example and demonstrate that the GKC mechanism can interpret the similar phenomenon of silica vapor-pressure-dependent growth of face-centered cubic (FCC) digenite nanocrystals in atmospheric pressure chemical vapor deposition (APCVD). In addition, due to the inertness of Cu, we designed two sets of experiments and for the first time determined the critical vapor pressures for silica sheath initialization and crystal shape maintenance.

Experimental Section

The Cu−S system has a complex phase diagram.[27] However, the only stable solid form of the Cu−S compound is FCC−digenite with an S atomic ratio of 33.4−36.6% above 507 °C. Thus, the synthesis temperature is set to be 750 °C. Gray-green CuCl powder containing about 2.5 wt % of water (2.5%-CuCl) was purchased from the Beijing Chemical Factory, China. Heat treatment at 240 °C in a vacuum results in anhydrous CuCl (An-CuCl). A mixture of An-CuCl and Si powder with a molar ratio of 3.6:1 (CuCl−Si) is used as the $SiCl_4$ source. No reaction is found to occur after 30 min treatment of the mixture at 300 °C, and there is still about 30% of CuCl left unreacted after 30 min of treatment at 350 °C. Such mild reactivity makes the mixture a suitable source of $SiCl_4$ in our experiments.

The apparatus and its temperature profile at 750 °C are shown in Scheme 1. All experiments were carried out in a quartz tube

* To whom correspondence should be addressed. E-mail: ydli@tsinghua.edu.cn.
† Tsinghua University.
‡ Institute of Physics.

10.1021/jp062346n CCC: $33.50
Published on Web 07/01/2006

SCHEME 1. Scheme of the Apparatus and Its Temperature Profile at 750 °C

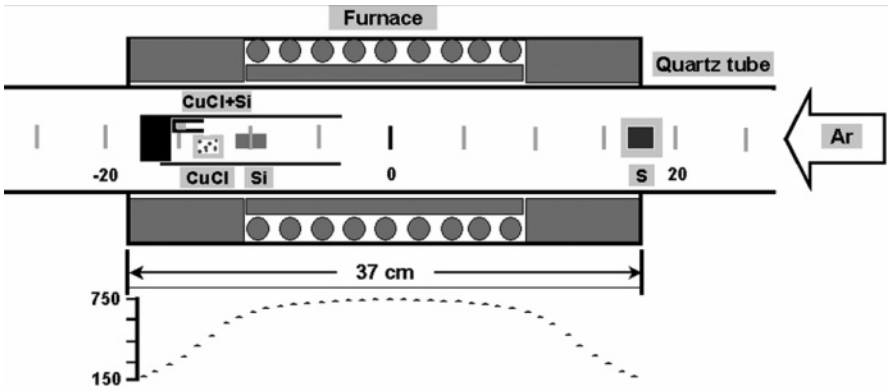

(scales drawn for positioning), which was placed in a 37 cm long horizontal tube furnace. A one-end-sealed ceramic tube was used as the crucible containing CuCl−Si to avoid direct exposure of the precursors to water vapor. An 11 cm long, one-end-sealed, thinner quartz tube was used to put the Si(100) substrates and two crucibles containing CuCl−Si (50 mg, −15.2 to −14.7 cm) and 2.5%-CuCl (or An-CuCl, 100 mg, −14.0 to −12.5 cm). Employment of this tube guarantees the best use of $SiCl_4$ to prevent incorporation of oxygen into the digenite crystals. The crucible containing sulfur (premelted before put into the system) was put at the position 17.0−19.0 cm. Water vapor was introduced into the reaction atmosphere through pinholes under careful control of the source temperatures. Two sets of experiments were carried out. One employed An-CuCl as the precursor to determine the critical water vapor pressure for sheath initialization. The other employed 2.5%-CuCl as the precursor to determine the water vapor pressure necessary to maintain the shape control of nanosheets or nanowires. We first put "24.0" at the right edge of the furnace. After evacuating and washing with argon flow, the system was filled with argon to atmospheric pressure and the argon flow was adjusted to 100 cm^3 (STP) min^{-1}. Then the furnace temperature was elevated to 600 °C in 20 min and then to 750 °C in 8 min. Finally, we moved the large quartz tube to the right so that "18.0" was now at the right edge of the furnace. The deposition lasted for 20 min. After that the furnace was allowed to cool to room temperature before the samples were taken out.

The samples were characterized by a LEO 1530 scanning electron microscope (SEM) and a Hitachi model H-800 transmission electron microscope (TEM) with a tungsten filament at an accelerating voltage of 200 kV.

Results

SEM I: Silica Sheath Initialization. An-CuCl powder is used in the first set of experiments, so that silica vapor pressure is solely controlled by water vapor introduced into the system. The results are summarized in Figure 1. As shown in Figure 1a, when the water vapor pressure is only $1P_0$ ($P_0 = 12$ Pa at room temperature), the silica vapor pressure is too low to affect the growth of digenite crystals; therefore, the crystals possess clear facets and show no preferred growth direction. When the water vapor pressure is elevated to $3P_0$, silica sheathes begin to form on digenite crystals, resulting in predominantly irregular microcrystals still with no preferred growth direction, see Figure 1b. Shape control only occurs when the water vapor pressure is enhanced to $5P_0$, as shown in Figure 1c. The products are mainly submicrorods with layered structure. Therefore, the critical water vapor pressure at the given conditions necessary for initialization of shape control is about $5P_0$.

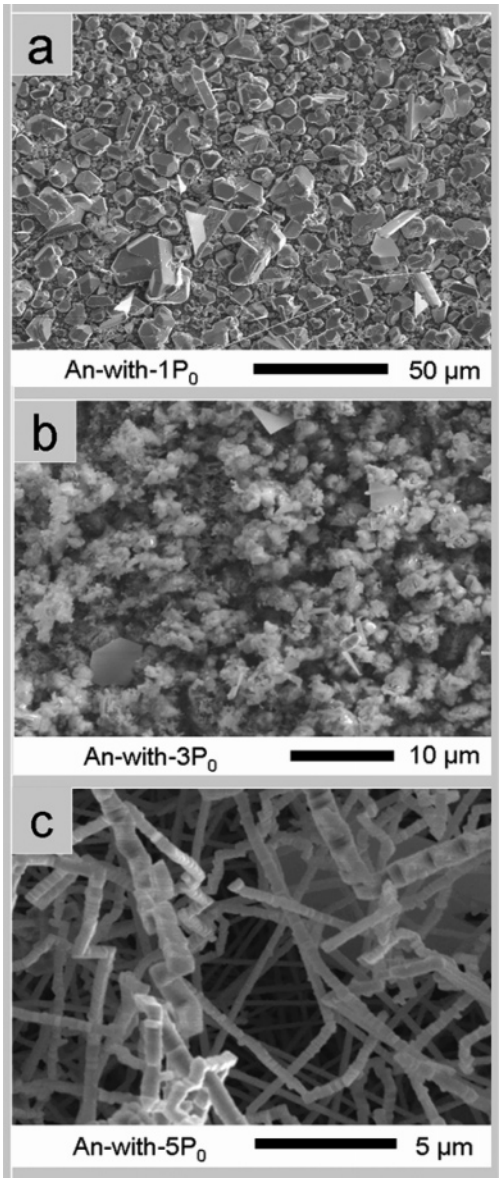

Figure 1. SEM images of digenite crystals grown from An CuCl powder under different water vapor pressures: (a) $1P_0$, (b) $3P_0$, and (c) $5P_0$.

SEM II: Silica Sheath Maintenance. 2.5%-CuCl is used in the other set of experiments to generate a peak water vapor pressure that is necessary for silica sheath initialization. However, the water vapor pressure quickly drops to the level determined by the water vapor introduced into the system; thus,

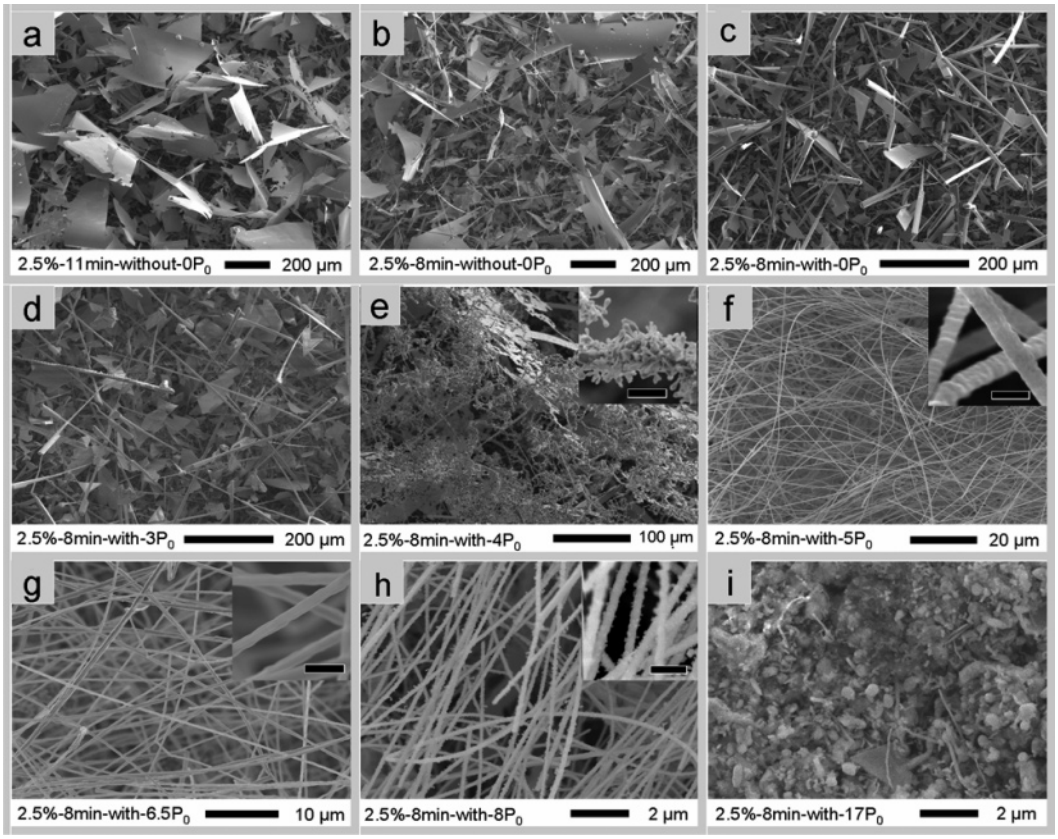

Figure 2. SEM images of digenite crystals grown from 2.5%-CuCl powder under different vapor pressures. "With" and "without" refer to whether a mixed powder of anhydrous CuCl and Si is used to supply $SiCl_4$. "8 min" means the deposition is conducted as soon as the furnace temperature is elevated to 750 °C, while "11 min" means the deposition is conducted 3 min later. Scale bars for insets of e−h are 5 μm, 500 nm, 1 μm, and 500 nm, respectively.

another important parameter, the water vapor pressure necessary to maintain shape control can be determined or estimated. The results are summarized in Figure 2. When 2.5%-CuCl is used, even without the aids of additional water vapor and $SiCl_4$ source, shape control can be achieved, resulting in nanosheets with more loss of water (see Figure 2a) and coexistence of nanosheets and submicrorods when more water is reserved (see Figure 2b). Iintroduction of $SiCl_4$ source seems to provide much higher silica vapor pressure because submicrorods begin to dominate in the final products (see Figure 2c). Introduction of water vapor up to $3P_0$ hardly affects the morphology (see Figure 2d). However, further enhancement to $4P_0$ abruptly results in irregular networks composed of microwires and nanorods as the main products (see Figure 2e and Supporting Information for higher resolution images). When the water vapor pressure reaches $5P_0$, the products suddenly and completely change to nanowires (see Figure 2f). Clearly layered structure can be easily identified in higher resolution images (see inset of Figure 2f). Further increasing the water vapor pressure to $6.5P_0$ blurs the layered structure (see Figure 2g), and an even further increase to $8P_0$ brings about some silica-sheathed nanoparticles growing on the nanowires (see Figure 2h). When the water vapor pressure is too high ($17P_0$), however, as shown in Figure 2i, the products are mainly composed of nanoparticles. Thus, in summary, shape control on digenite nanocrystals has been achieved by varying the silica vapor pressure. The successful synthesis of nanosheets even without the presence of additional water vapor and a $SiCl_4$ source demonstrates that a fairly low silica vapor pressure is enough to maintain the shape control of nanosheets. However, a significantly higher silica vapor pressure (corresponding to a water vapor pressure of $5P_0$) is required to maintain the shape control of nanowires.

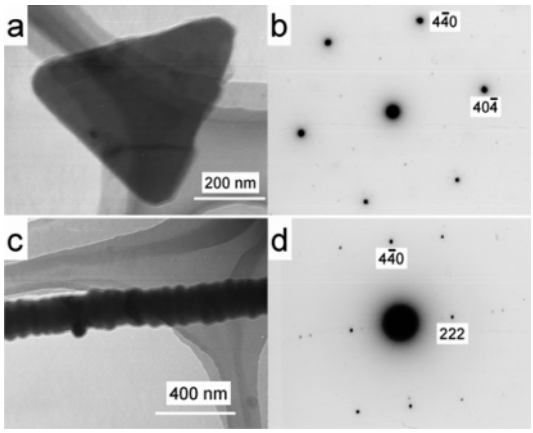

Figure 3. TEM images of (a) a nanosheet and (c) a nanowire. (b and d) Corresponding SAED patterns of the nanosheet and the nanowire, respectively.

TEM. The results of TEM characterizations on digenite nanosheets and nanowires are summarized in Figure 3. As revealed by the selected area electron diffraction (SAED) patterns, the nanosheet grows perpendicularly to the ⟨111⟩ direction, while the nanowire with a clearly layered structure (see Figure 3c) grows along the ⟨111⟩ direction. Therefore, along with enhancement of the silica vapor pressure, the silica sheathes act as not only the confiners to the growth of the cores, but also the controller to the growth directions. A kinetic competition must exist.

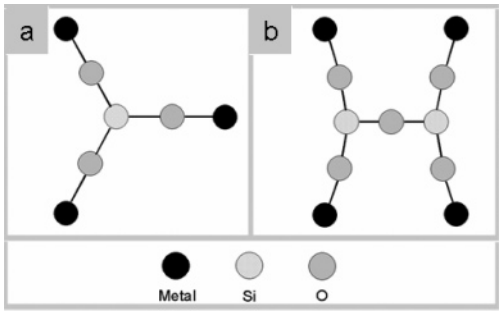

Figure 4. Two simplest modes for adsorbed silica species on metal sulfide crystals to determine a preferred surface: (a) a SiO_3 cluster on a triangle and (b) a Si_2O_5 cluster on a rectangle.

Discussion

Chemistry. We systematically studied the APCVD synthesis of a host of low-dimensional materials, including sulfides,[4,28a−h] silicates,[28i] silicides,[28h] and metals,[28j] from metal chloride precursors in the past 3 years. In our work on the synthesis of sulfides,[4,28a−h] the main reactions in similar chemical systems have been already discussed in detail. Most importantly, on the basis of the fact that the Si−O bond is significantly stronger than any other chemical bond that may form in the chemical system, we pointed out in ref 4a that (i) the stable chemical species in the final products should be metal sulfides and silica and (ii) the adsorption of silica species on metal sulfides cores is oxygen-bridged Si−(O)−metal−S type rather than sulfur-bridged O−Si−(S)−metal type. Here, in our experiments, the inner diameter of the one-end-sealed tube is just one-half of that of the outer large quartz tube. Thus, overestimation of the amounts of water and sulfur entering into the small tube will be one-fourth that carried by the argon flow, which gives a molar ratio of S:Si:O = 110:3:1 in the reaction atmosphere when the water vapor pressure is $5P_0$ (60 Pa at room temperature). Therefore, although water has been deliberately introduced into the system, the same conclusions can still be drawn for the chemical system discussed here.

General Introduction of GKC. Since the silica vapor-pressure-dependent growth behavior mentioned in the Experimental Section is quite similar to that observed in the SiO_2–Fe_7S_8 system,[4b] a brief review of the GKC mechanism responsible for the phenomenon may help to interpret the experimental results here. In that work we emphasized that the sheath initialization stage, which requires a high silica vapor pressure, is essential to determine the final shapes and growth directions of the products.[4b] As is well known, three spots determine a plane. Similarly, it requires at least three atoms in a specific surface of the core crystal to directly bond with silica species to determine a preferred adsorption surface for silica sheath formation. Therefore, the two simplest modes for adsorbed silica species to determine a preferred surface can be easily drawn as Figure 4 when the silicon atoms are sp^3 hybridized. As shown in Figure 4a, a SiO_3 cluster forms three bonds with metal atoms in a specific surface. If the structure is free of tension, the three metal atoms would lie on the three apexes of an equilateral triangle. As shown in Figure 4b, a Si_2O_5 cluster contains the fewest atoms among the silica species that can form four bonds with metal atoms in a specific surface. In this case the four metal atoms form a rectangle. In comparison, the latter structure includes more bonds between adsorbed silica species and the core material but requires more atoms to attend. Therefore, it is thermodynamically more favorable but kinetically more unfavorable than the former one. Thus, with the enhancement of the silica vapor pressure, the former may dominate at first while the latter one last. This mechanism may be called GKC, that is, kinetic competition between geometrical recognition of triangles and rectangles.

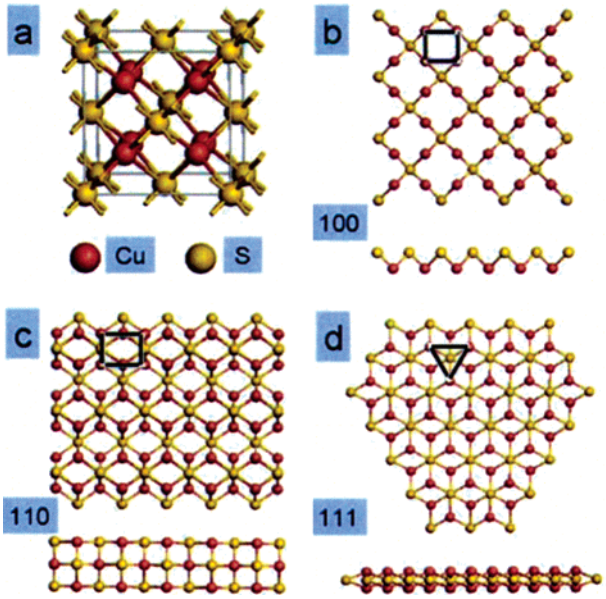

Figure 5. Structure of ideal FCC−Cu_2S crystal composed of only Cu−I atoms and free of defects. Both bird-view (upper parts) and side-view (lower parts) pictures are shown for (100), (110), and (111) surfaces. The rectangles and equilateral triangles composed of Cu atoms are highlighted in b for (100), c for (110), and d for (111) surfaces.

Crystal Structure of Digenite. We now explain the experimental results based on the crystal structure of digenite. According to literature,[29] two types of Cu atoms exist in the digenite crystal. One type, Cu−I, coordinates with four S atoms (bond length 2.415 Å, weaker bonding) and occupies equivalent positions of (0.25, 0.25, 0.25), while the other, Cu−II, coordinates with only three S atoms (bond length 2.277 Å, stronger bonding) and occupies equivalent positions of (0.333, 0.333, 0.333). They statically occupy about the same amounts of positions in the crystal. In addition, as high as about one-ninth of the Cu positions are point defects. Therefore, to solve the problem, we may start with ideal FCC−Cu_2S crystals composed of only Cu−I atoms and free of defects. The crystal structure and atom arrangements in the low index surfaces (100), (110), and (111) are shown in Figure 5.

GKC in the SiO_2–Cu_2S System. Equilateral triangles with a side length of 3.944 Å can be found only on (111) surfaces of an ideal FCC−Cu_2S crystal. In contrast, rectangles can be found on both (100) and (110) surfaces. However, the former may be too small (2.788 × 2.788 Å), and high tension is expected for adsorption of Si_2O_5 clusters. Thus, the latter, which has a proper size of 2.788 × 3.944 Å, may act as a much better adsorption site for Si_2O_5 clusters.

When an ideal FCC−Cu_2S crystal enclosed with two equivalent (111) surfaces and six equivalent $(1\bar{1}0)$ surfaces is viewed along the ⟨111⟩ direction, it will possess the same symmetry with 3C−Fe_7S_8 crystals and the same GKC mechanism may work on both of the crystals, giving rise to similar silica vapor-pressure-dependent growth behaviors, as shown in Scheme 2. Growth of silica-sheathed nanocrystals will have four stages. They are the crystal seed formation stage, the sheath initialization stage, the stage when critical coverage of silica sheath on specific surface(s) is reached, and the last stage when the final products are obtained. Now let us discuss these in detail.

SCHEME 2. Scheme of Silica Vapor-Pressure Dependence Growth of Silica-Sheathed Metal Sulfides Nanocrystals under the GKC Mechanism[a]

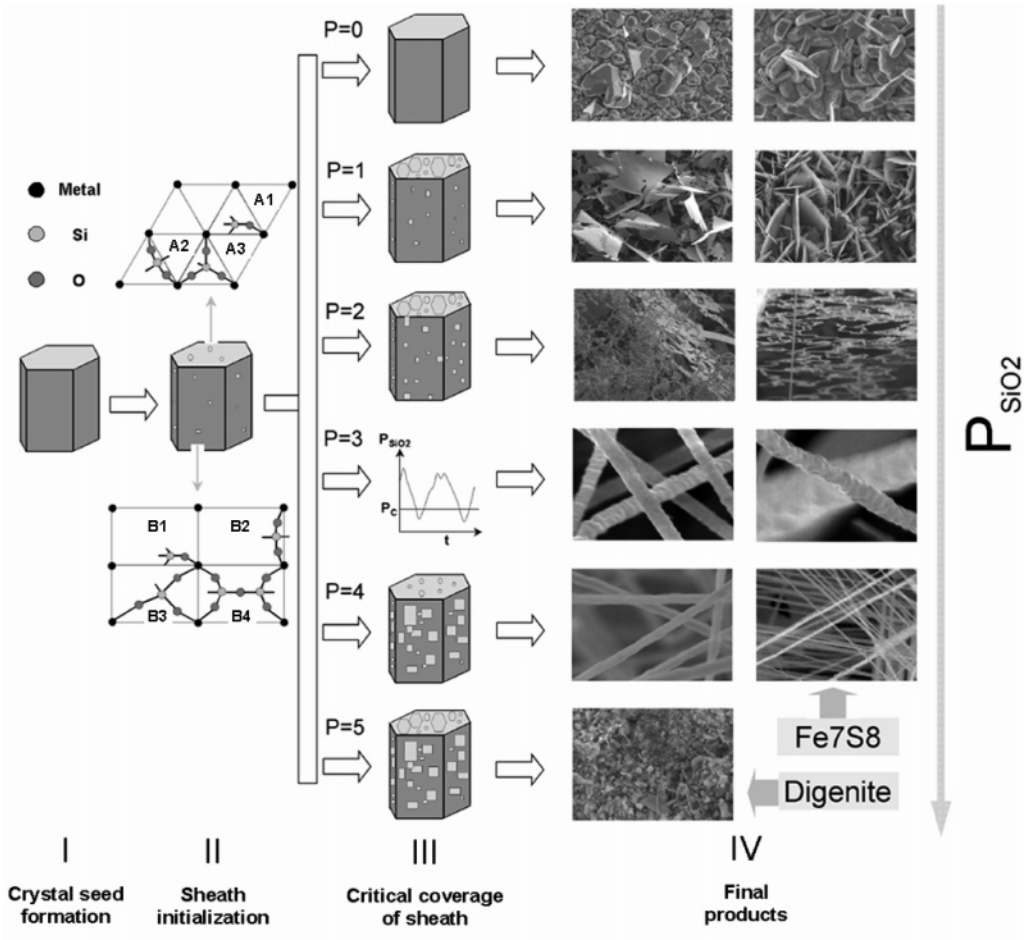

[a] This is effective when Case A3 is thermodynamically more favorable than case B3. Numbers 0−5 represent the levels of silica vapor pressure in an increasing sequence. Curve drawn after $P = 3$ shows fluctuation of silica vapor pressure around the critical level for the growth of nanowires.

(1) First, the crystal seeds must be formed to serve as adsorption beds for silica species. As shown in the two figures corresponding to $P = 0$ in Scheme 2, although freely grown digenite and 3C−Fe_7S_8 crystals have different shapes, due to the difference between their intrinsic symmetries, the maximum exposed surfaces of them all have hexagonal symmetry. Since the chance for silica sheath formation on a specific surface depends on the overall area of the surface, this situation should favor formation of nanosheets for both of them.

(2) At the second stage silica species begin to adsorb on the surfaces of the crystal seeds. Here only those silica species that have finally formed at least three bonds with the surfaces are important because not only are they much more stable, but also the crystal is growing. Since the coverage of silica sheath is still low at this stage, silica sheath forms mainly through the weaker metal−oxygen bonds rather than much stronger Si−O bonds. Therefore, this stage is a slow process, which requires a high silica vapor pressure, so that growth of the silica sheath can compete with that of the crystal.

(3) When a critical coverage of silica sheath on a specific surface is reached, the growth process enters into the third stage, which is characterized by fast sheath growth on the surface with the aid of Si−O bonds. When case A3 is thermodynamically more favorable than case B3, as shown in Scheme 2, the GKC mechanism works. In addition, according to the GKC mechanism, the preferred surfaces for silica sheath formation should be dependent on the silica vapor pressure: when the silica vapor pressure is low ($P = 1$), the surfaces should be those with hexagonal symmetry (A planes) and the products are nanosheets; when the silica vapor pressure is high ($P = 4$), the surfaces should be those that possess rectangle units (B planes) and the products are nanowires; and when the silica vapor pressure is too high ($P = 5$), silica sheaths will form almost simultaneously on all surfaces and the products are predominantly nanoparticles.

(4) When the silica vapor pressure is but moderate ($P = 2$ and 3), two intermediate morphologies have been observed for both of the crystals. In the case of $P = 2$, when the silica sheaths have reached the critical coverage on A surfaces, its coverage on the B planes may have also reached a fairly high level, so that the growth of silica sheaths on the B planes may be sustained with the aid of the silica sheaths on A planes. Such products should be nanosheets that suffer further restrictions from the sides, that is, zigzag nanowire/nanobelts growing in the hexagonal plane. In the case of $P = 3$, nanowires with rough surfaces are obtained. This interesting phenomenon may be attributed to the fluctuation of the silica vapor pressure around the critical level (P_C) necessary to sustain the growth of the sheath. Once the pressure drops below P_C, the inner crystal will outgrow the sheath. In this temporarily free growth the B planes that had been passivated before begin to grow. However, as long as the pressure returns to above P_C, sheath growth will soon catch up with the growth of the inner core and the restriction on the crystal growth is set up again. In this process a nod forms on the nanowire. Obviously when the silica vapor

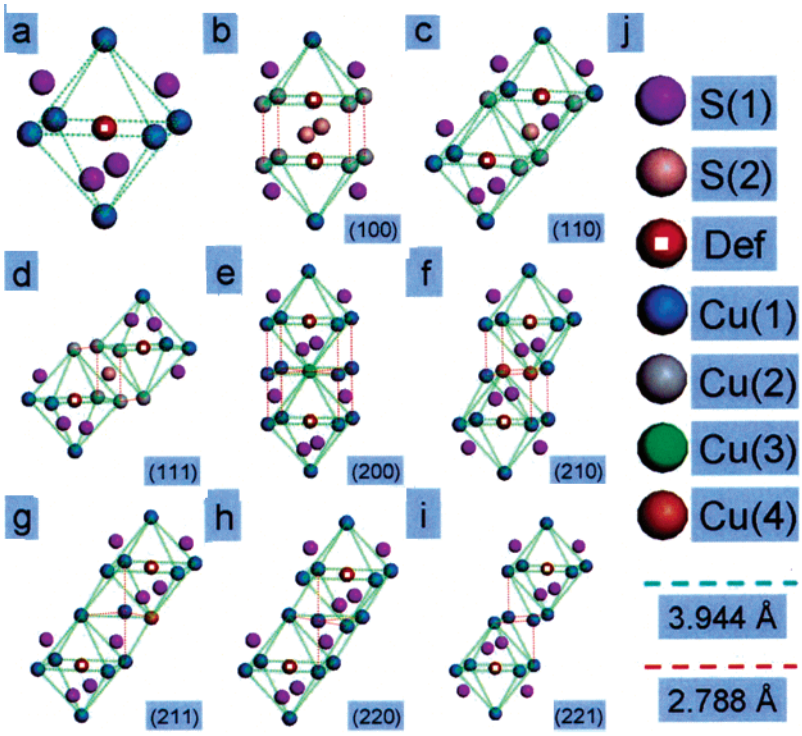

Figure 6. Structures of (a) point defect and (b−i) point defect pairs before relaxation. (100), (110), etc., indicate relative positions of the two point defects in the Cu sublattice. The atoms drawn here include (1) Cu point defects, (2) S atoms that originally coordinate with the defects, (3) Cu atoms that coordinate with at least two of the S atoms. S(1) originally coordinates with one Cu at the defect site and S(2) with two. Cu(1) coordinates with two S(1), Cu(2) with one S(1) and one S(2), Cu(3) with four S(1), and Cu(4) with three S(1). According to the supposed GKC mechanism, equilateral triangles enclosed by three green lines are responsible for the growth of nanosheets perpendicular to the ⟨111⟩ direction, while rectangles composed of two green lines and two red lines are responsible for the growth of nanowires along the ⟨111⟩ direction.

pressure is elevated so that it is always higher than P_C, the surfaces of the products will become smother, as demonstrated by the experimental results shown in the case of $P = 4$ in Scheme 2.

Possible Mechanism for Formation of Nanosheets of FCC−Digenite. Digenite has a FCC structure, which possesses eight equivalent (111) planes with an octahedral arrangement, as shown in Figure 6a. If all these planes were simultaneously covered by silica sheath in the case of $P = 1$ shown in Scheme 2, the products would be nanoparticles rather than nanosheets. This does not happen, probably because the silica vapor pressure ($P = 1$) is still low. In such situations silica sheath coverage will rather reach the critical level on one of the (111) planes of an octahedral digenite crystal first rather than simultaneously on all eight (111) planes. Since stage III is a much faster process than stage II, the preemptive plane may soon be solely covered by silica sheath before sheath coverage on the other seven planes reaches the critical level. The situation is drawn in Scheme 3. For simplicity, a cube is drawn instead of an octahedron to represent the digenite crystal. We may now attribute the formation of nanosheets to the positive feedback between the imbalance of silica sheath coverage on different planes and the net mass diffusion associated with the imbalance. As shown in Figure 1a, the fact that all the digenite crystals possess clear facets means the surface diffusion of adsorbed cuprite sulfide species is fairly active under the experimental conditions. Supposing the cube is not covered by silica sheath, then all six planes are equivalent and no net mass diffusion will occur among these planes. However, when one plane, the A plane as illustrated in Scheme 3, is solely covered by silica sheath, net mass transport occurs. The A plane acts as an extremely strong adsorption bed (through Si−O bonds) for silica species, so that silica sheath grows fastest on this plane. Consequently, the adjacent B planes will "feel" a lower silica vapor pressure than $P = 1$. In comparison, the A′ plane, which is furthest from the A plane, will be less affected than the B planes. Thus, silica sheath will grow faster on the A′ plane than on the B planes. Obviously similar discussions on mass transport of cuprite

SCHEME 3. Scheme of the Formation Process of Digenite Nanosheets when $P = 1$[a]

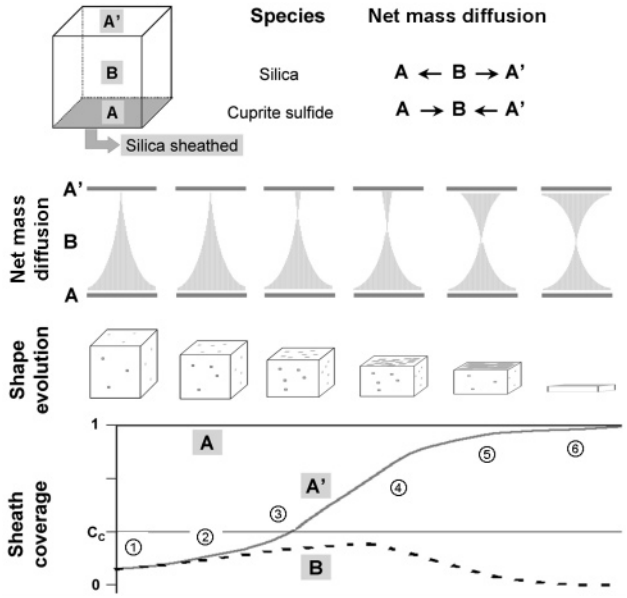

[a] Density of the net mass transport is represented by the width of the shaded parts. C_C is the critical coverage, after which sheath growth is featured with fast growth through strong Si−O bonds rather than slow growth through metal−oxygen bonds as before.

sulfide species will lead to the conclusion of faster growth of digenite crystals on the B planes. Lastly, the cooperation of faster silica sheath growth on the A and A′ planes and faster crystal growth on the B planes results in the shape evolution from the original cubes to the final products of nanosheets.

Point Defect Effect. We now deal with the influence of defects on kinetic competition. Once a point defect occurs, as shown in Figure 6a, the bonds associating with the four S atoms, which originally coordinate with the Cu atom that occupies the defect position, should be strengthened. Obviously the most influenced Cu atoms would be those coordinated with at least two of the S atoms. Such Cu atoms should be more Cu−II-like (stronger Cu−S bonds than Cu−I) and act as stronger adsorption sites for silica species than those further away from the defect. As shown in Figure 6a, the six Cu−II-like atoms form eight equilateral triangles (or eight (111) planes) suitable for formation of nanosheets. Thus, it is clear that point defects should favor growth of nanosheets. Since digenite is highly defective, the structures of point defect pairs are also drawn in Figure 6b−i. In most cases the (111) planes still predominate, except when the relative position of the defect pair is (100) in the Cu−I sublattice, as shown in Figure 6b. However, since the point defects are too close in this structure, the formation energy is probably much higher than for the others, so that its total influence may be negligible.

Conclusions

In summary, this paper reports shape control synthesis of digenite nanosheets and nanowires growing perpendicularly by varying the silica vapor pressure. The phenomenon can be explained well by the mechanism of GKC. Since units of an equilateral triangle or a rectangle with proper sizes can be singled out in a variety of materials with hexagonal, FCC, tetragonal, and orthorhombic structures, we expect our simple model to be helpful to predict and achieve shape control on more functional materials.

Acknowledgment. We are thankful for financial support from NSFC (20131030) and the state key project of fundamental research for nanomaterials and nanostructures (2003CB716901).

Supporting Information Available: Higher resolution SEM images of 2.5%-8min-with-4P_0, SEM image of 2.5%-12min-with-0P_0, and XRD patterns 2.5%-11min-without-0P_0, 2.5%-8min-with-0P_0, and 2.5%-8min-with-5P_0 (PDF). This material is available free of charge via the Internet at http://pubs.acs.org.

References and Notes

(1) Zhang, Y. F.; Tang, Y. H.; Wang, N.; Yu, D. P.; Lee, C. S.; Bello, I.; Lee, S. T. *Appl. Phys. Lett.* **1998**, *72*, 1835.

(2) Zhang, Y. F.; Tang, Y. H.; Wang, N.; Lee, C. S.; Bello, I.; Lee, S. T. *Phys. Rev. B* **2000**, *61*, 4518.

(3) Zhang, R. Q.; Lifshitz, Y.; Lee, S. T. *Adv. Mater.* **2003**, *15*, 635.

(4) (a) Zhang, H. X.; Ge, J. P.; Li, Y. D. *Chem. Vapor. Deposit.* **2005**, *11*, 147. (b) Zhang, H. X.; Ge, J. P.; Wang, J.; Wang, Z.; Yu, D. P.; Li, Y. D. *J. Phys. Chem. B* **2005**, *109*, 11585.

(5) Wang, S. H.; Yang, S. H.; Dai, Z. R.; Wang, Z. L. *Phys. Chem. Chem. Phys.* **2001**, *3*, 3750.

(6) Tang, C. C.; Bourgeois, L.; Bando, Y.; Golberg, D. *Chem. Phys. Lett.* **2003**, *382*, 374.

(7) Lai, H. L.; Wong, N. B.; Zhou, X. T.; Peng, H. Y.; Au, F. C. K.; Wang, N.; Bello, I.; Lee, C. S.; Lee, S. T.; Duan, X. F. *Appl. Phys. Lett.* **2000**, *76*, 294.

(8) Hu, J. Q.; Ma, X. L.; Shang, N. G.; Xie, Z. F.; Wong, N. B.; Lee, C. S.; Lee, S. T. *J. Phys. Chem. B* **2002**, *106*, 3823.

(9) Shi, W. S.; Zheng, Y. F.; Wang, N.; Lee, C. S.; Lee, S. T. *Chem. Phys. Lett.* **2001**, *345*, 377.

(10) May, S. J.; Zhang, J. G.; Wessels, B. W.; Lauhon, L. J. *Adv. Mater.* **2005**, *17*, 598.

(11) Persson, A. I.; Larsson, M. W.; Stenström, S.; Ohlsson, B. J.; Samuelson, L.; Wallenberg, L. R. *Nat. Mater.* **2004**, *3*, 677.

(12) Dick, K. A.; Deppert, K.; Märtensson, T.; Mandl, B.; Samuelson, L.; Seifert, W. *Nano Lett.* **2005**, *5*, 761.

(13) Peng, X. G.; Manna, L.; Yang, W. D.; Wickham, J.; Scher, E.; Kadavanich, A.; Alivisatos, A. P. *Nature* **2000**, *404*, 59.

(14) Puntes, V. F.; Krishnan, K. M.; Alivisatos, A. P. *Science* **2001**, *291*, 2115.

(15) Sun, Y. G.; Xia, Y. N. *Science* **2002**, *298*, 2176.

(16) Yang, J.; Xue, C.; Yu, S. H.; Zeng, J. H.; Qian, Y. T. *Angew. Chem., Int. Ed.* **2002**, *41*, 4697.

(17) Shi, H. T.; Qi, L. M.; Ma, J. M.; Wu, N. Z. *Adv. Funct. Mater.* **2005**, *15*, 442.

(18) Zhang, S.; Peng, L. M.; Chen, Q.; Du, G. H.; Dawson, G.; Zhou, W. Z. *Phys. Rev. Lett.* **2003**, *91*, 256103.

(19) Zhang, S.; Chen, Q.; Peng, L. M. *Phys. Rev. B* **2005**, *71*, 014104.

(20) Kong, X. Y.; Wang, Z. L. *Nano Lett.* **2003**, *3*, 1625.

(21) Kong, X. Y.; Wang, Z. L. *Appl. Phys. Lett.* **2004**, *84*, 975.

(22) Yang, R. S.; Ding, Y.; Wang, Z. L. *Nano Lett.* **2004**, *4*, 1309.

(23) Saponjic, Z. V.; Dimitrijevic, N. M.; Tiede, D. M.; Goshe, A. J.; Zuo, X. B.; Chen, L. X.; Barnard, A. S.; Zapol, P.; Curtiss, L.; Rajh, T. *Adv. Mater.* **2005**, *17*, 965.

(24) Schmidt, V.; Senz, S.; Gösele, U. *Nano Lett.* **2005**, *5*, 931.

(25) Manna, L.; Wang, L. W.; Cingolani, R.; Alivisatos, A. P. *J. Phys. Chem. B* **2005**, *109*, 6183.

(26) (a) Zhang, R. Q.; Chu, T. S.; Cheung, H. F.; Wang, N.; Lee, S. T. *Phys. Rev. B* **2001**, *64*, 113304. (b) Zhang, R. Q.; Chu, T. S.; Cheung, H. F.; Wang, N.; Lee, S. T. *Mater. Sci. Eng. C* **2001**, *16*, 31. (c) Chu, T. S.; Zhang, R. Q.; Cheung, H. F. *J. Phys. Chem. B* **2001**, *105*, 1705.

(27) Massalski, T. B. *Binary Alloy Phase Diagrams*; ASM International: USA, 1990; p 1467.

(28) (a) Ge, J. P.; Li, Y. D. *Chem. Commun.* **2003**, 2498. (b) Ge, J. P.; Li, Y. D. *Adv. Funct. Mater.* **2004**, *14*, 157. (c) Ge, J. P.; Wang, J.; Zhang, H. X.; Li, Y. D. *Chem.*—Eur. J. **2004**, *10*, 3525. (d) Li, X. L.; Ge, J. P.; Li, Y. D. *Chem.*—Eur. J. **2004**, *10*, 6163. (e) Ge, J. P.; Wang, J.; Zhang, H. X.; Wang, X.; Peng, Q.; Li, Y. D. *Adv. Funct. Mater.* **2005**, *15*, 303. (f) Ge, J. P.; Wang, J.; Zhang, H. X.; Wang, X.; Peng, Q.; Li, Y. D. *Chem.*—Eur. J. **2005**, *11*, 1889. (g) Ge, J. P.; Wang, J.; Zhang, H. X.; Wang, X.; Peng, Q.; Li, Y. D. *Sens. Actuators B* **2006**, *113*, 937. (h) Zhang, H. X.; Ge, J. P.; Wang, J.; Li, Y. D. *Nanotechnology* **2006**, *17*, S253. (i) Wang, J.; Ge, J. P.; Zhang, H. X.; Li, Y. D. *Small* **2006**, *2*, 257. (j) Wang, J.; Zhang, H. X.; Ge, J. P.; Li, Y. D. *J. Phys. Chem. B* **2006**, *110*, 807.

(29) Gasymov, G. B.; Asadov, Ju. G.; Gusejnov, G. G.; Gezalov, M. A.; Belov, N. V. *Doklady Akademii Nauk SSSR* **1978**, *239*, 846.